# Impact of plasma oxidation on structural features of human epidermal growth factor

**Maksudbek Yusupov[1], Jan-Wilm Lackmann[2,3], Jamoliddin Razzokov[1], Surendra Kumar[4], Katharina Stapelmann[2,5] and Annemie Bogaerts[1]**

[1] Research Group PLASMANT, Department of Chemistry, University of Antwerp, Universiteitsplein 1, B-2610 Antwerp, Belgium

[2] Institute for Electrical Engineering and Plasma Technology, Ruhr-University Bochum, D-44780 Bochum, Germany

[3] ZIK plasmatis at Leibniz Institute for Plasma Science and Technology, INP Greifswald e.V. Felix-Hausdorff-Str. 2, 17489 Greifswald, Germany

[4] College of Pharmacy, Gachon University of Medicine and Science, Hambakmoeiro 191, Yeonsu-gu, Incheon City, 21936, Korea

[5] Department of Nuclear Engineering, North Carolina State University, 2500 Stinson Dr, Raleigh, NC 27607, USA

E-mail: maksudbek.yusupov@uantwerpen.be

## Abstract

We perform computer simulations supported by experiments to investigate the oxidation of an important signaling protein, i.e., human epidermal growth factor (hEGF), caused by cold atmospheric plasma (CAP) treatment. Specifically, we study the conformational changes of hEGF with different degrees of oxidation, to mimic short and long CAP treatment times.

Our results indicate that the oxidized structures become more flexible, due to their conformational changes and breakage of the disulfide bonds, especially at higher oxidation degrees. MM/GBSA calculations reveal that an increasing oxidation level leads to a lower binding free energy of hEGF with its receptor.

These results help to understand the fundamentals of the use of CAP for wound healing vs cancer treatment at short and longer treatment times.

## Keywords

cold atmospheric plasma, plasma treatment, protein oxidation, molecular dynamics

## Abbreviations

| | |
|---|---|
| CAP | − cold atmospheric plasma |
| DBD | − dielectric barrier discharge |
| hEGF | − human epidermal growth factor |
| hEGFR | − human epidermal growth factor receptor |
| AA | − amino acid |
| DFTB | − density functional tight−binding |
| MD | − molecular dynamics |
| ROS | − reactive oxygen species |
| RNS | − reactive nitrogen species |
| FTIR | − Fourier transform infrared |
| SASA | − solvent accessible surface area |
| CD | − circular dichroism |
| PCA | − principle component analysis |
| RMSD | − root mean square deviation |
| MM/GBSA | − molecular mechanics generalized Born surface area |
| *A. dest* | − distilled water |

# 1. Introduction

Cold atmospheric plasmas (CAPs) are investigated for several medical applications. The inactivation of bacteria [1] and improved wound healing [2] are already studied in clinical trials. Three types of plasma sources, an Ar plasma torch, an Ar plasma jet and a dielectric barrier discharge (DBD) operated in air [2-4] are accredited as medical devices in Germany, each with its own benefits and limitations. A major research effort is devoted to the promotion of wound healing in chronic wounds. These wounds, typically associated with diabetes, are a major health concern due to their high occurrence in the population, long healing time, and associated high costs. Cell culture studies [5] and clinical trials [6] show promising results towards wound reduction or closure using relatively short plasma treatment times between 45 s and 2 min [7]. Another growing application of CAPs is the inactivation of cancer cells [8]. While short treatment times associated with wound healing seem to induce no permanent damage [9], cancer treatments are performed at significantly higher plasma exposure times. First results are promising, as plasma treatment inactivates various cancer lines in cell culture experiments [10], xenografts [11], and patient studies [12].

Due to the complex nature of both wound healing and cancer, investigating the effect of plasma is challenging. Nevertheless, several studies show that treated cells have upregulated antioxidative protection systems, both after short treatment times [13] as well as periodic short treatments in an elongated time frame [14].

One system that seems highly interesting in both wound healing and cancer is the epidermal growth factor receptor (EGFR) and one of its ligands, the epidermal growth factor (EGF). EGFR is known to be involved in several cancer types [15], because an overproduction or overstimulation of EGFR has a severe impact on the cell cycle by inducing proliferation, survival and differentiation [16]. Furthermore, a variant of EGFR in humans is described as a favorable marker for breast cancer diagnosis [17]. Besides EGFR, its ligand EGF is also investigated concerning its role in various cancer types [18]. EGF is a small 53 amino acid (AA) protein [16], which binds to EGFR thanks to its specific structure. While EGF does not seem to have cancer-inducing capabilities, it triggers chemotaxis, mitogenesis, motogenesis and cytoprotection, allowing the promotion of cancer growth [19]. However, exactly these triggers are highly beneficial in wound healing, making EGF the typical double-edged sword in cancer treatment [20].

EGF is probably present both during the application of plasma to wounds as well as during cancer treatment. Investigating the impact of plasma treatment on EGF is therefore of great interest to improve our understanding how plasma interacts with several components of the human body, relevant for both wound healing and cancer treatment. Indeed, it is well known that CAP treatment can have a strong impact on proteins by over-oxidizing disulfide bonds [21], structure denaturing [22], as well as introducing modifications at various AAs [23].

Besides wet-lab approaches, *in silico* simulations offer a valuable tool to gain insights into molecular processes difficult to observe experimentally [24]. In the context of plasma medicine, a number of simulation studies were carried out to obtain atomic-level insights into the mechanisms of plasma-biomolecule interactions [25]. By means of reactive molecular dynamics (MD) simulations, including density functional tight-binding (DFTB), the effect of CAP oxidation on different bio-surfaces was investigated, such as the interaction of CAP-generated reactive oxygen species (ROS) with bacterial cell wall components [26], structural modifications of the skin barrier [27] and P-glycoprotein [28] induced by OH radicals, as well as their interaction with water [29], DNA [30] and biofilm components [31]. In general, the interaction of ROS with the above mentioned model systems always leads to the breaking and formation of some bonds, eventually resulting in the modification of these systems, as revealed by the simulations. In [32], quantum mechanical MD simulations were applied to investigate the interaction of oxygen atoms with phosphatidylcholine, i.e., a single cell membrane lipid. Furthermore, combined DFTB and non-reactive MD simulations were used to study the ROS oxidation of the head groups and lipid tails in the cell membrane [33]. Using model lipid-like layers as found on cell membranes, non-

reactive MD simulations were carried out to study the sputtering process of these layers, induced by CAP-generated Ar ion bombardment [34]. Non-reactive MD simulations were also applied to investigate the permeation of ROS through oxidized and non-oxidized cell membranes, including the synergistic effect of plasma oxidation and electric field [35] and the hampering effect of cholesterol [36]. Finally, the effect of lipid oxidation on the phosphatidylserine translocation across the cell membrane, which plays a vital role in apoptosis signaling, was studied [37].

In the present study we carry out non-reactive MD simulations to investigate the effect of oxidation on the human EGF (hEGF) protein. As treatment times vary significantly between wound healing and cancer inactivation (see above), we consider a range of different oxidation degrees, mimicking both short and long treatment times, to cover both the application of wound healing and cancer treatment. To support the performed simulations, we use the results of Fourier transform infrared (FTIR) spectroscopy. Using the theoretical analysis of the solvent accessible surface area (SASA) and data from literature [23], we create the oxidized hEGF proteins through modification of specific AA residues. The effect of these modifications on the protein is then investigated applying MD simulations. As only the modifications affecting the binding efficacy of hEGF to EGFR are important for signal transduction, we focus on the overall structure. To complement the protein structure analysis, we perform circular dichroism (CD) spectroscopy on the treated hEGF, again to support the simulations by analyzing if any structural changes occurred in the hEGF structure. Finally, docking simulations and free energy calculations are performed between hEGF and the EGFR domain to obtain insight in their binding affinity.


## 2. Computational details

As mentioned above, hEGF is a small protein consisting of 53 AA residues with three disulfide bonds formed between the cysteine residues (see Fig. S1 in the Supporting Information). The crystal structure of this protein is available in the Protein Data Base (PDB ID: 2KV4 [38], sequence available from UniProtKB #Q6QBS2_HUMAN [39]). As a model system in our simulations we use the hEGF protein surrounded with water. After equilibration of this model system at 300 K in the NPT ensemble for 300 ns, we apply oxidation to the system through modification of the AA residues. In this study we employ three model systems for oxidized hEGFs, which are called OX1, OX2 and OX3. Since the creation of these oxidized structures is based on our modeling and, in part, experimental results (see below), we assume that the oxidation degrees used in our simulations for OX1, OX2 and OX3 can be broadly correlated to treatment times of various length. These model systems are also equilibrated at 300 K using an NPT ensemble for 800 ns. Details about the equilibration of the native and oxidized hEGFs with water layer surrounding them, are given in the Supporting Information.

All MD simulations are carried out using the GROMACS 5.1 package [40], applying the GROMOS54A7 force field [41]. In the case of the oxidized hEGFs, i.e., with the modified AAs, we use the parameters of the GROMOS force field obtained from [42]. The last 30 ns of the equilibration is used for analysis of the results. Specifically, we calculate the solvent accessible surface area (SASA) of each AA residue in the native hEGF, to find out the highly exposed AAs to the solvent (see the Supporting Information for more details). These AAs are then used to create the oxidized hEGF structures (see details in section 4). We also carry out principle component analysis (PCA) to examine the structural modifications. For computation of the secondary structure of the proteins, we use the secondary structure assignment program STRIDE [43], by averaging the data obtained from 100 snapshots of the MD trajectory taken at every 300 ps from the last 30 ns. To compare how much the oxidized hEGFs are structurally altered from the native one, we perform alignment of these structures using the final snapshots of the MD simulations, applying VMD visualizing tool [44]. Finally, we calculate the root mean square deviations (RMSDs) of the alpha carbons of the native and oxidized hEGFs, to determine the flexibility of these structures.

As mentioned above, to mimic the different CAP treatment times, we modify the native hEGF to create various oxidized states (which we call OX1, OX2 and OX3), using the results of the SASA analysis, in combination with the chemical reactivity and modification of the AAs, given in [23]. In addition, FTIR analysis is used to provide a general idea if the chosen modifications are valid. Detailed information about the hEGF modification procedure is given in section 4. Table 1 summarizes the applied modifications of the AAs in the oxidized structures.

**Table 1.** *AAs involved in the creation of various oxidized states of the hEGF protein. The chemical structures of these (un)modified AAs are given in Table S1 of the Supporting Information.*

| AA in native hEGF | modified AA in oxidized hEGF |
|---|---|
| methionine (MET) | methionine sulfoxide |
| cysteine (CYS) | cysteic acid |
| tryptophan (TRP) | 6-hydroxytryptophan |
| tyrosine (TYR) | 3,4-dihydroxyphenylalanine |
| histidine (HYS) | 2-oxo-histidine |
| proline (PRO) | pyroglutamic acid |
| lysine (LYS) | allysine |
| glutamine (GLN) | 4-hydroxyglutamine |
| valine (VAL) | 3-hydroxyvaline |
| leucine (LEU) | 4-hydroxyleucine |

Using the AAs listed in Table 1, we modify 23, 38 and 53% of the (53) AAs of the native hEGF to create the oxidized hEGF structures. These oxidation degrees were chosen based on data obtained with the plasma source as described in [21], as explained in detail in section 4.

We also perform docking simulations using the Z-DOCK v2.3 program [45] to estimate the binding affinities between native and oxidized hEGF proteins with the hEGF receptor (hEGFR, PDB ID: 1IVO [46]). Additionally, we apply the molecular mechanics generalized Born surface area (MM/GBSA) method [47] to calculate binding free energies of native and oxidized hEGF proteins with the hEGFR. Details of the docking simulations and free energy calculations are given in the Supporting Information.

# 3. Experimental details

**Dielectric Barrier Discharge (DBD) source**

The DBD used for the experiments is described in detail in [48, 49]. In short, a copper electrode with a diameter of 1 cm is enclosed in an $Al_2O_3$ dielectric. A grounded metal plate is used as counter electrode. The source is driven by -13 kV at a frequency of 300 Hz. Ambient air is used as the process gas. The distance between the electrode and the treated samples was kept constant at 1 mm. An in-depth characterization of the source can be found in [49, 50]. Various reactive oxygen and nitrogen species are generated by the discharge, as shown by 0D simulations as well as experiments. The source is capable of producing *e.g.* atomic oxygen, ozone, hydroxyl as well as nitric oxide and other RNS [49].

**Sample preparation and treatment conditions**

Commercially available hEGF (#10605HNAE250, Life Technologies GmbH) is suspended in *A. dest* with a final concentration of 50 µg/ml (equaling about 8.33 µM) in 100 µM $KH_2PO_4$. Samples of 20 µl are placed on IR-transmittable Si-wafers and treated for 45 s to 600 s. For the FTIR measurements, the samples are dried and stored in a desiccator until measurement. For CD

spectroscopy, 10 treated samples are collected, stored at -80 °C and pooled for a final volume of 200 μl prior to measurements. No temperature increase is observed after 10 min of treatment.

**FTIR spectroscopy**

The dried samples are measured using an FTIR-microspectrometer Spotlight 200 (PerkinElmer). Spectra are recorded in the range of 750 to 4000 cm$^{-1}$ in transmission mode with a spectral resolution of 4 cm$^{-1}$. For each sample, 10 measurement points are chosen and 64 spectra are acquired at each point for a total of 640 spectra per sample. Afterwards, the spectra are baseline corrected, normalized using a Euclidean normalization, and the average as well as standard error is calculated. For details, see [51]. Spectral features are annotated using [52]. All measurements are performed in triplicate.

**CD spectroscopy**

The pooled samples are stored on ice prior to measurement. Spectra are acquired on a J-815 Spectrometer (Jasco) instrument in a range of 250 to 200 nm with a spatial resolution of 4 nm. The spectra are background corrected using buffer-only spectra measured before and after each replicate. To take into account various efficiencies in sample collection after DBD treatment, the protein concentrations are determined using commercially available Bradford Assay (Roti Nano-Quant, Roth). Afterwards, the spectra are smoothed using Savitzky-Golay filter with a binning of 50, the molar ellipticities are calculated, and the averages as well as standard error calculated for the three replicates.

# 4. Results and discussion

**Oxidized hEGF proteins by modification of specific AAs**

As mentioned in section 2, we used the results of SASA and the chemical reactivity and modification of AAs deduced from [23] for modification of specific AAs (see below) in order to create the oxidized hEGF structures (OX1, OX2 and OX3). To support the performed simulations, hEGF protein was treated for three different treatment times from short (45 s) over long (300 s) to very long (600 s). While no direct correlation between the simulated oxidation states and treatment times are possible, we tried to approximate low, high, and even higher modified states as applied in our simulations. To this aim, we chose a treatment time used for clinical application (45 s), as well as two treatment times known to induce high levels of modifications in proteins, as shown in [21].

Takai *et al.* studied the chemical modifications of AAs, as well as their reactivity, by individually treating them with CAP for 5 and 10 min [23]. Based on high-resolution mass spectrometry, they observed chemical modifications of 14 AAs (among the 20 naturally occurring AAs) after plasma treatment. Moreover, they found that some AAs, i.e., MET and CYS, have higher chemical reactivity than other AAs. Although the experimental conditions of our study and the study of Takai *et al.* are somewhat different, we assume that we can still deduce the chemical reactivity and oxidation products of AAs obtained in [23], since both CAP sources generate a cocktail of RONS, which results in both cases in the oxidation of AAs. In our model system we have 18 types of AAs (see Fig. 1 below). Based on the results of Takai *et al.* [23], we excluded asparagine (ASN), serine (SER), aspartic acid (ASP), glycine (GLY) and alanine (ALA) from the oxidation, and we used the following order for the reactivity of the other AAs in our modifications (in order of decreasing reactivity): MET → CYS → TRP → TYR → HIS → the rest of the AAs. We also excluded glutamic acid (GLU), isoleucine (ILE) and arginine (ARG) from the modifications, as we either do not have the GROMOS force field parameters [42] for these modifications or the available parameters do not correspond to the modifications obtained in [23] for these AAs. Hence, we modified 10 types of AAs (or in total 28

AAs) of the native hEGF, which contain newly formed C-OH, S=O or C=O bonds (see Table S1 in the Supporting Information).

As is clear, the native hEGF contains more than one type of the same AAs (*e.g.*, $CYS_6$, $CYS_{14}$, $CYS_{20}$, etc., see Fig. 1) and the selection of the initial AAs for modification depends on the SASA results. The results of the SASA analysis for each AA residue of the native hEGF are given in Fig. 1.
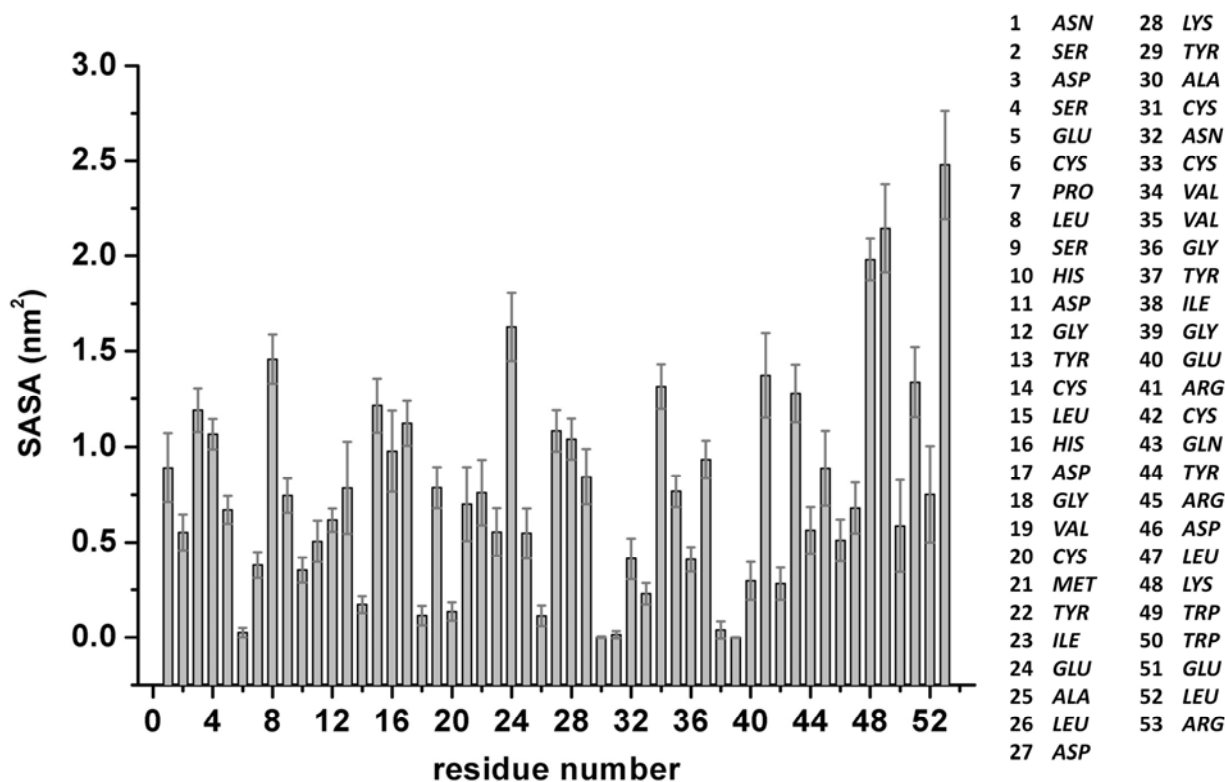


| 1 | ASN | 28 | LYS |
|---|---|---|---|
| 2 | SER | 29 | TYR |
| 3 | ASP | 30 | ALA |
| 4 | SER | 31 | CYS |
| 5 | GLU | 32 | ASN |
| 6 | CYS | 33 | CYS |
| 7 | PRO | 34 | VAL |
| 8 | LEU | 35 | VAL |
| 9 | SER | 36 | GLY |
| 10 | HIS | 37 | TYR |
| 11 | ASP | 38 | ILE |
| 12 | GLY | 39 | GLY |
| 13 | TYR | 40 | GLU |
| 14 | CYS | 41 | ARG |
| 15 | LEU | 42 | CYS |
| 16 | HIS | 43 | GLN |
| 17 | ASP | 44 | TYR |
| 18 | GLY | 45 | ARG |
| 19 | VAL | 46 | ASP |
| 20 | CYS | 47 | LEU |
| 21 | MET | 48 | LYS |
| 22 | TYR | 49 | TRP |
| 23 | ILE | 50 | TRP |
| 24 | GLU | 51 | GLU |
| 25 | ALA | 52 | LEU |
| 26 | LEU | 53 | ARG |
| 27 | ASP | | |

***Figure 1.*** *Theoretical analysis of the solvent accessible surface area (SASA) of each AA in the native hEGF structure. The AA residues are listed at the right.*

It is obvious that among the 53 AA residues, some are highly exposed to solvent (*e.g.*, $ARG_{53}$, $TRP_{49}$, $LYS_{48}$, $GLU_{24}$, $SER_9$), whereas other AAs (*e.g.*, $GLY_{18}$, $LEU_{26}$, $ALA_{30}$, $ILE_{38}$, $GLY_{39}$) have less access to solvent. Moreover, all $CYS_6$, $CYS_{14}$, $CYS_{20}$, $CYS_{31}$, $CYS_{33}$, $CYS_{42}$ residues also have less contact with solvent due to their location in the core of the structure (cf. Fig. S1(a)). However, as discussed above, due to the high chemical reactivity of CYS, we need to take these residues into account, even if they are less exposed to solvent. Nevertheless, the choice of the initial CYS residues for modification will depend on their surface area given in Fig. 1, i.e., $CYS_{33}$ and $CYS_{42}$ (bound to each other, see Table 2) will be modified before $CYS_{14}$ and $CYS_{31}$, etc. In addition, FTIR data (Fig. 2) can be used to gain insight into some chemical changes after plasma treatment. While no structural information can be obtained from FTIR data due to the drying of the samples prior to measurements, some changes in the spectra can be used to gain insight into some chemical modifications occurring after plasma treatment. Therefore, FTIR is a convenient way to investigate if certain decisions during the simulation are valid.
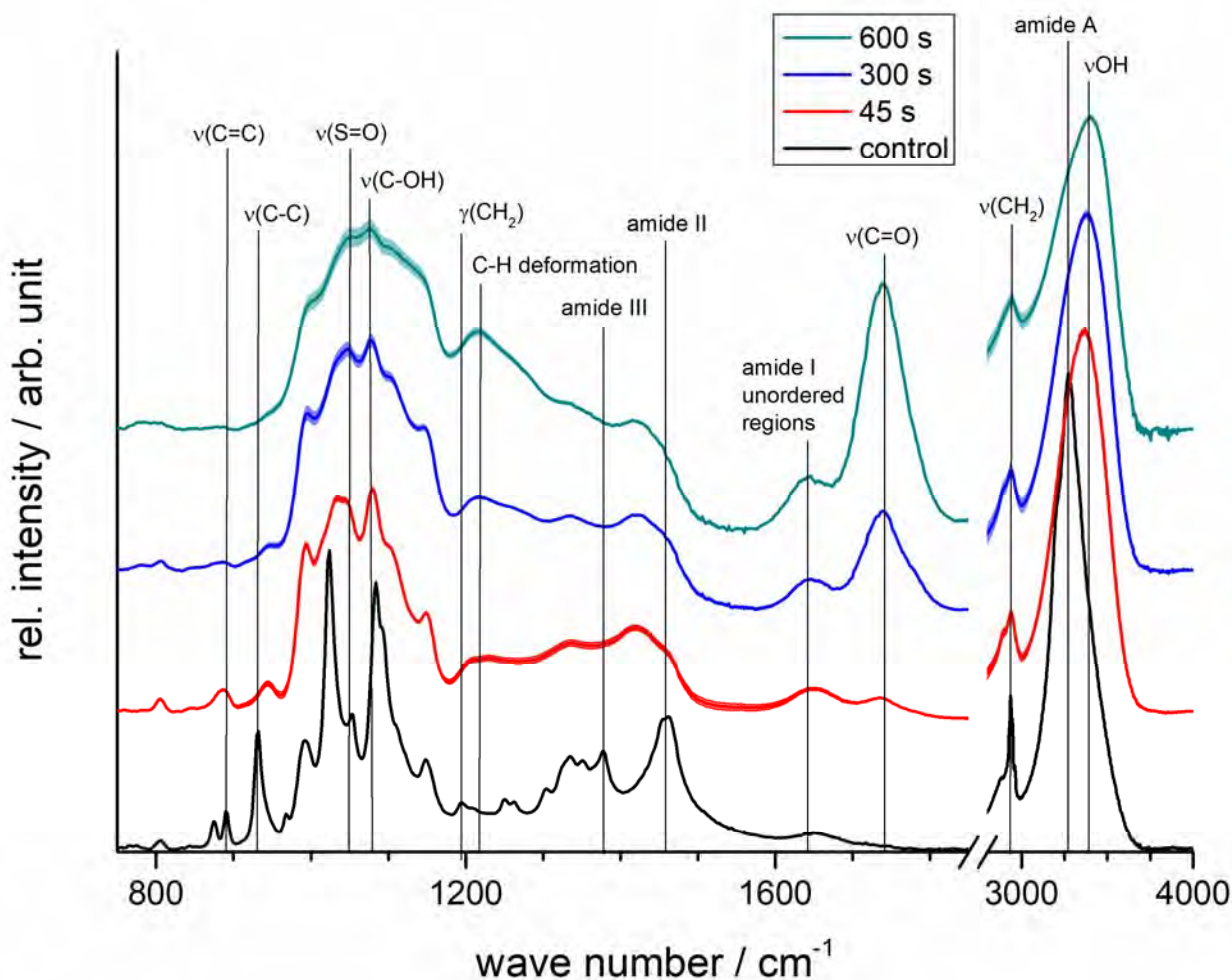
***Figure 2.*** *FTIR spectra of plasma-treated hEGF. The mean and standard error (shaded area) for each treatment time are shown. Spectra were stacked with a fixed factor of 0.03 to increase readability.*

The plasma treatment leads to chemical changes in the hEGF protein, indicated by the FTIR data. Multiple bands show a peak broadening after treatment, whereas new signals occur or are shifted in the spectrum. One well-known signal at 1068 cm$^{-1}$ increases with plasma treatment time, which can be annotated as $\nu$(S=O), indicating the presence of oxidized sulfur residues. Furthermore, a strong signal occurs at 1750 cm$^{-1}$, indicating the formation of oxidized carbons, as this signal can be annotated as $\nu$(C=O). Furthermore, peak broadening is observed for the TRP double signals at 1300 cm$^{-1}$ and 1040 cm$^{-1}$. Such shifts can be induced by an incomplete addition of a hydroxyl groups to the TRP residue. While structural changes cannot be directly identified due to the drying process during sample generation, the broadening of amide bands is typically described as a marker for thermodynamically instable α-helices [53], which might be induced by the presence of chemically modified AAs interrupting the normal AA interactions. While no good assessment of amide A is possible due to the overlay with the $\nu$(OH) signal, it would be expected that part of the very strong $\nu$(OH) signal stems from the underlying broadened amide I band, as indicated by its slight shoulder corresponding to the original amid A signal. In addition, broadening of amide I and II can easily be observed.

Taken together, FTIR measurements indicate that S=O and OH groups are already introduced after 45 s of treatment, which is in good agreement with previous studies [21, 51]. This means that we should mostly concentrate on modifications of the thiol-containing AAs, MET and CYS (see Table 2 below as well as Table S1 in the Supporting Information). In the case of 300 s and

longer, the intensity of the ν(C-OH) signal is lower, whereas the C=O formation is increased. These results, taken together with competition assays conducted by Takai *et al.* [23], indicate that besides thiol oxidation, simulated changes should be introduced to HIS and LYS.

Thus, based on the combined results of FTIR spectroscopy, SASA analysis and the reactivity and modification of AAs deduced from [23], we defined which residues are modified, to create the oxidized hEGF structures with different percentages, as detailed in Table 2.

***Table 2.*** *AAs modified at different levels of oxidation, to create the oxidized hEGFs (OX1, OX2 and OX3). The choice of the specific AAs for modification is based on the results of [23], in combination with SASA results and in part FTIR data.*

| Oxidation | AAs to be modified and their positions in hEGF | Percentage of oxidation (%) |
|---|---|---|
| OX1 | LEU$_8$, TYR$_{13}$, HIS$_{16}$, MET$_{21}$, TYR$_{22}$, TYR$_{29}$, CYS$_{33}$, TYR$_{37}$, CYS$_{42}$, TYR$_{44}$, TRP$_{49}$, TRP$_{50}$ | 23 |
| OX2 | **AAs of OX1 +** HIS$_{10}$, CYS$_{14}$, LEU$_{15}$, VAL$_{19}$, CYS$_{31}$, VAL$_{34}$, GLN$_{43}$, LYS$_{48}$ | 38 |
| OX3 | **AAs of OX2 +** CYS$_6$, PRO$_7$, CYS$_{20}$, LEU$_{26}$, LYS$_{28}$, VAL$_{35}$, LEU$_{47}$, LEU$_{52}$ | 53 |

As is clear, in each oxidation case (i.e., OX1, OX2 or OX3) we oxidized a pair of CYS residues (i.e., each to cysteic acid, see Table S1), which were bound together prior to modification via disulfide bonds (cf. Fig. S1). More specifically, for OX1 we oxidized CYS$_{33}$ and CYS$_{42}$; for OX2, we oxidized in addition also CYS$_{14}$ and CYS$_{31}$; finally for OX3 we also oxidized CYS$_6$ and CYS$_{20}$ (see Table 2). The oxidation of these CYS residues to cysteic acids leads to the dissociation of the disulfide bonds between these residues. These bonds are important, since they help to stabilize the structure of the protein. Hence, breakage of these bonds leads to conformational changes, which we indeed observed below.

## Conformational changes in the oxidized hEGF proteins

Figure 3 illustrates the time evolution of the RMSD of the alpha carbons for each oxidation state, as well as for native hEGF.
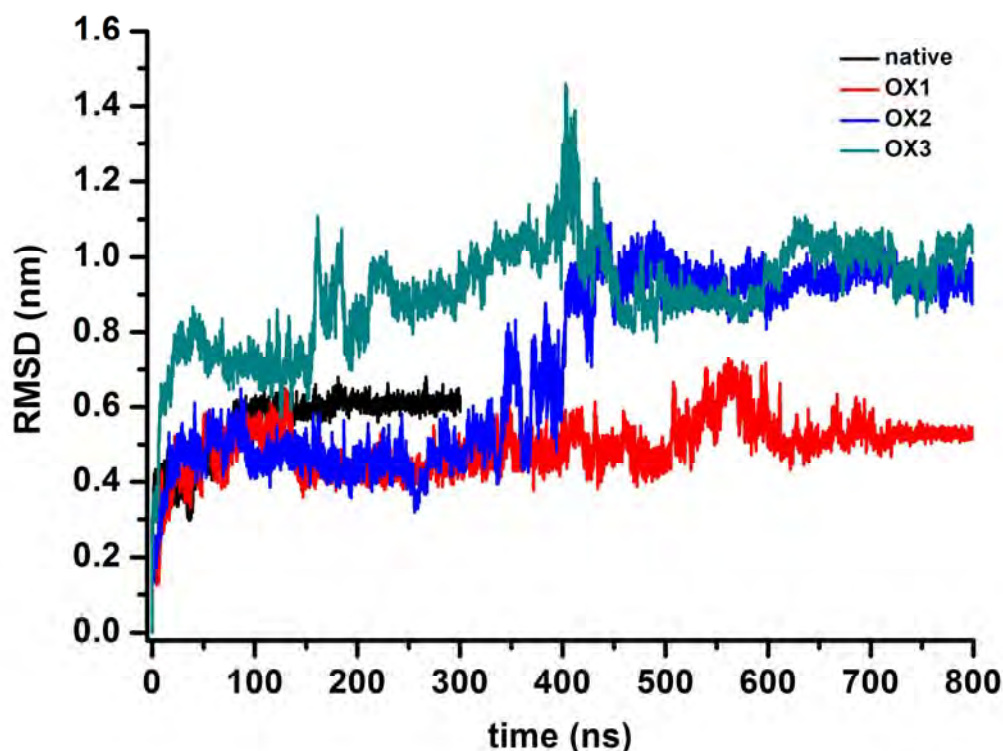
***Figure 3.*** *MD simulations: RMSD of the alpha carbons of the native (black) and oxidized hEGF proteins (red, blue and cyan, respectively).*

As is clear, the native hEGF reaches its equilibration after ~100 ns and stays stable in the rest of the simulation time, yielding an RMSD fluctuating around 0.6 nm. In contrast, the oxidized hEGF structures obtain their stability at a much longer time, i.e., at around 650 ns. Moreover, an increasing oxidation level leads to higher fluctuations of the RMSD (see OX2 and OX3). This indicates that the oxidized structures become more flexible, which is due to their conformational changes, as well as the breakage of the disulfide bonds (see above). The conformational change in the case of OX1 is lower compared to OX2 and OX3 (as will be illustrated below), which is also obvious from their relative RMSD values, i.e., 0.5 nm (for OX1) versus 1 nm (for OX2 and OX3), see Fig. 3.

To further support the RMSD results, we performed a PCA for the native and oxidized hEGF structures, where the collective motion of the alpha carbons is studied by plotting the projection of the first eigenvector (representing the direction of the highest motion) versus the projection of the second eigenvector (representing the second highest motion). In other words, the PCA results show the total phase space that each protein is able to occupy. The results of the PCA are presented in Fig. 4.
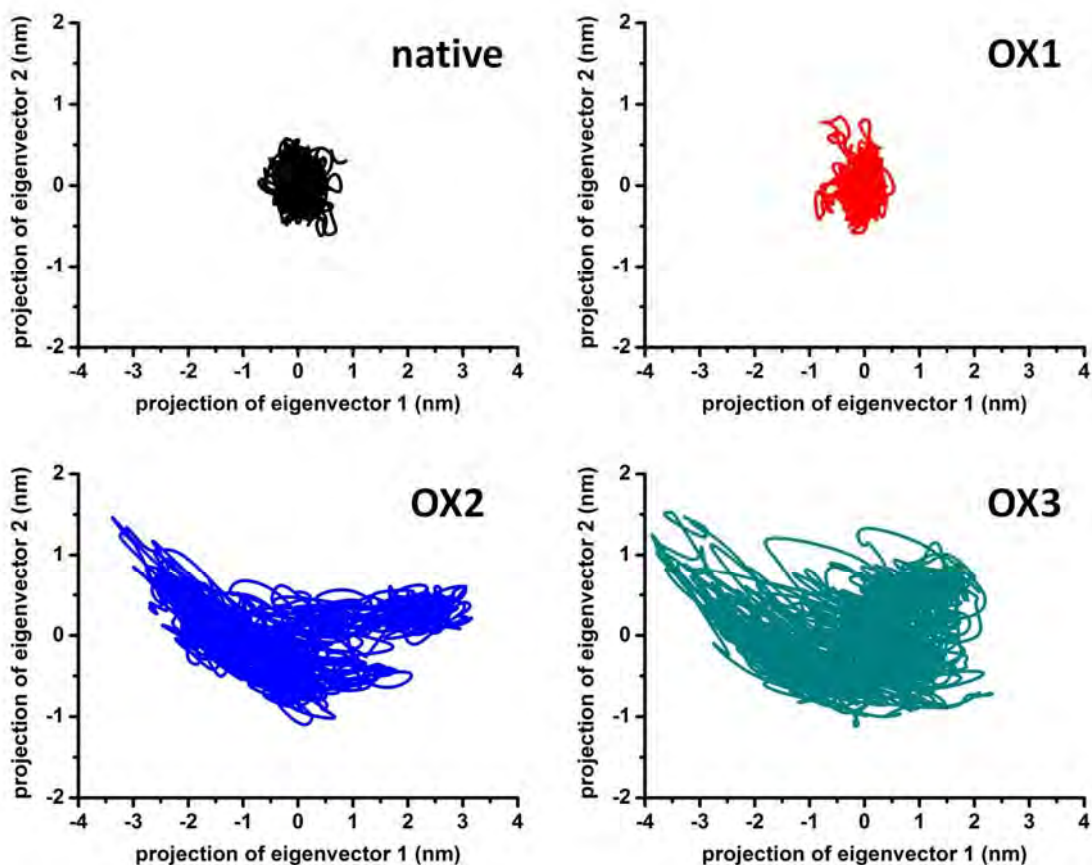
**Figure 4.** *PCA results obtained for the native and oxidized hEGF structures, collecting the data from the last 30 ns of the simulations.*

In the case of OX1 we do not see significant effect of oxidation on the overall structure, i.e., the phase space occupied by OX1 is almost the same as for the native hEGF, despite the fact that one of the disulfide bonds (out of three) is already broken. This indicates that this low oxidation degree does not significantly affect the structural stability and flexibility, and does not lead to drastic conformational changes. On the other hand, in the OX2 and OX3 structures we clearly see higher structural fluctuations, indicating a higher flexibility of these systems. OX3 corresponds to the highest oxidation degree, where all three disulfide bonds are dissociated, thereby having the highest occupation in the phase space. This is also clear from Fig. 5, where the alignments of the oxidized structures with the native hEGF are shown.
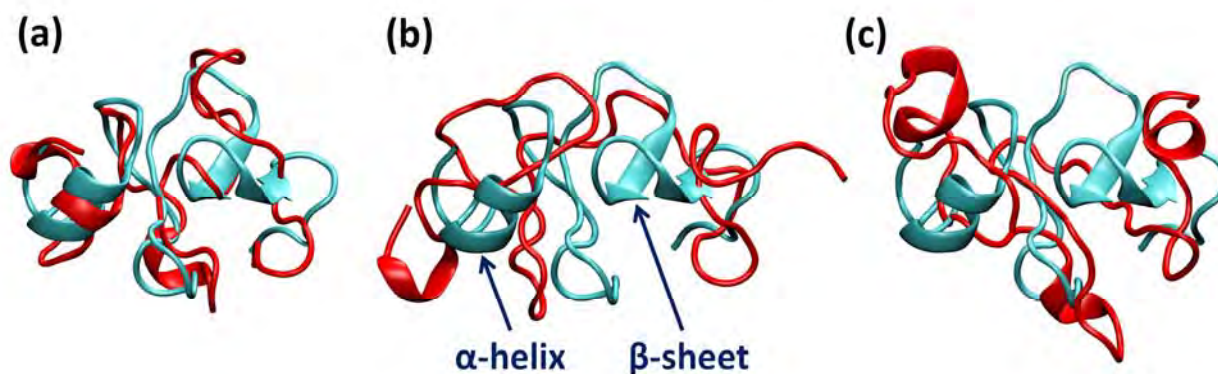


**Figure 5.** *Alignment of the OX1 (a), OX2 (b) and OX3 (c) structures (red) with the native hEGF (cyan). The last snapshots of the MD simulations are used to illustrate the conformational changes of the oxidized hEGFs compared to the native hEGF.*

As is obvious from Fig. 5, the OX1 structure exhibits a better alignment with the native hEGF, whereas OX2 and OX3 show significant deviations. Moreover, in all oxidation cases the structures lose their β-sheet conformations, which are responsible for the structural stability. Furthermore, the helical structures also start to form at random sites, which is more visible in the case of OX3. Thus, we can conclude that a higher level of oxidation may lead to completely new conformations in the hEGF protein (see Fig. 5). The latter is also clear from Table 3, presenting the results of the secondary structure analysis for the native and oxidized hEGFs.

*Table 3. Secondary structure analysis of the native and oxidized hEGFs. The values given denote the relative occurrence (in %) of the various conformations.*

| structure | α-helix | $3_{10}$-helix | π-helix | β-sheet | β-bridge | turn | coil |
|-----------|---------|----------------|---------|---------|----------|------|------|
| Native | 11.2 | 0.6 | 0.0 | 10.9 | 2.3 | 48.7 | 26.4 |
| OX1 | 7.6 | 3.9 | 0.0 | 0.0 | 0.0 | 65.6 | 22.8 |
| OX2 | 0.0 | 1.4 | 0.0 | 0.0 | 8.0 | 66.5 | 24.1 |
| OX3 | 7.4 | 3.4 | 5.8 | 0.5 | 4.3 | 44.9 | 33.7 |

These structural modifications, leading to conformational changes, obviously affect the binding free energies of the hEGFs with their hEGFRs. Indeed, as shown in Figs. S2 and S3 and listed in Tables S2, S3 and S4, our docking simulations and MM/GBSA calculations revealed that the binding free energies of native and modified hEGFs with their hEGFR are -105.15, -71.21, -63.85 and -49.49 kcal/mol for the native, OX1, OX2 and OX3 structures, respectively, showing that higher oxidation causes a lower interaction. For more details about the docking and MM/GBSA results, see the Supporting Information.

To support our simulation results on the impact of treatment on the hEGF structure, we performed CD spectroscopy (Fig. 6).
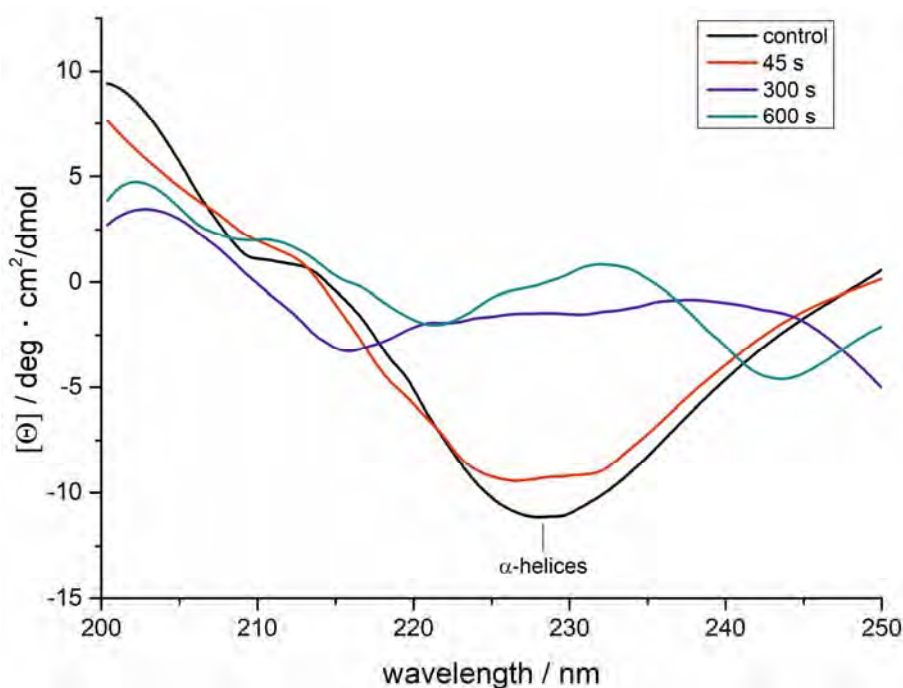


*Figure 6. Secondary structure analysis of plasma-treated hEGF by CD spectroscopy.*

The CD data indicate that 45 s of treatment cause only slight alterations in the hEGF secondary structure compared to control spectrum, whereas longer treatments (300 s and 600 s) result in a stronger disturbance of the secondary structure of the hEGF, especially in the region around 225

nm, which indicates a strong impact on the α-helices. Although our computational and experimental results cannot directly be compared, due to the complex nature of the plasma which is difficult to describe by modeling, our simulation results on the conformational changes are overall in good qualitative agreement with the results of the CD spectroscopy. Due to the nature of DBD treatment, a significant decrease in pH can be expected, especially during longer treatment times and considering the low buffer concentrations necessary for CD spectroscopy. However, crystallization data on hEGF showed that all relevant structural features are retained by hEGF at low pH compared to physiological pH [54]. Narhi et al. investigated the relevance of the disulfide bonds in hEGF on its secondary structure by CD spectroscopy at pH 3 [55]. While the presented spectra do not perfectly agree, most likely due to different buffers as well as pH conditions, it is apparent that disulfide bonds play a major role in determining the secondary structure of hEGF. Taking into account the strong impact of DBD treatment on disulfide bonds and its capability to oxidize disulfide bonds to e.g. cysteine sulfonic acid (R-SO$_3$H) [56], differences in CD spectra might be due to the formation of sulfur-containing residues all with a negative charge, thereby further promoting unfolding of the structure, as shown for longer treatment times. The additional introduction of C=O bounds, as indicated by FTIR spectroscopy, might also assist in the unfolding process.

Thus, we can conclude from our simulation results that the lower oxidation (i.e., OX1) has comparatively less effect on the binding affinity of hEGF with its receptor (see above). This most likely does not strongly influence the signaling pathways in a cell, and thereby the cell proliferation, which might explain why CAP at short treatment times is beneficial for chronic wound healing [4]. On the other hand, higher oxidation of hEGF (i.e., OX2 and OX3) causes clearly less interaction with its hEGFR, which most probably causes a disturbance of the signaling pathways in a cell, ultimately leading to a disruption of the cell proliferation. This might explain the effect of CAP at longer treatment times on inhibiting cancer cell proliferation and even cancer cell death [8, 57].

## 5. Conclusions

We show that a low amount of modified amino acids caused by CAP treatment does not cause significant structural changes in hEGF, and thus, has comparatively lower impact on the hEGF interaction with hEGFR. So we might expect only limited disturbance of the signaling pathways and hence of the cell proliferation. This is favorable in e.g., wound healing, where treatment with CAP at short treatment times or mild conditions indeed does not (or little) affect the cell proliferation, while being effective in decontamination of pathogens [58]. On the other hand, analysis of the results for a higher oxidation degree (used to approximate longer CAP treatment times) of hEGF shows a significant effect on the structural conformation and the binding affinity with EGFR, and this will most probably cause inhibition of the cell growth or proliferation. This might be important in cancer treatment by means of CAP, as higher doses of oxidation arrest the cell growth, leading to apoptosis or even necrosis [59].

It should be noted that CAP treatment of cells is a complex process, and the interaction of signaling proteins with their receptors is only one of the steps of the entire mechanism of cell proliferation. Nevertheless, our study might contribute to a better understanding of one of the possible mechanisms of (inhibition of) cell proliferation, by means of oxidation of signaling proteins. In the next step, the impact of plasma-treated hEGF should be analyzed in vitro to complement the simulations and the current experimental data, e.g., by applying hEGF to cell culture and compare the cellular response. In addition, experimental validation of the MM/GBSA simulations should be performed using e.g., artificial membrane systems populated with hEGFR.

Our study is of particular importance for biomedical applications of CAP, but it is also of more general interest for other therapies which cause oxidation (e.g., photodynamic therapy).

## Supporting Information

The Supporting Information contains the computational details, i.e., the model systems and their preparation. It also contains four Supporting Tables and three Supporting Figures as well as an extended discussion of the simulations results.

## Acknowledgements

## References

[1]    G. Fridman, G. Friedman, A. Gutsol, A. B. Shekhter, V. N. Vasilets, A. Fridman, Plasma Processes and Polymers 2008, 5, 503.

[2]    G. Isbary, W. Stolz, T. Shimizu, R. Monetti, W. Bunk, H.-U. Schmidt, G. Morfill, T. Klämpfl, B. Steffes, H. Thomas, Clinical Plasma Medicine 2013, 1, 25.

[3]    C. Ulrich, F. Kluschke, A. Patzelt, S. Vandersee, V. Czaika, H. Richter, A. Bob, J. Von Hutten, C. Painsi, R. Hügel, Journal of wound care 2015, 24, 196.

[4]    S. Emmert, F. Brehmer, H. Hänßle, A. Helmke, N. Mertens, R. Ahmed, D. Simon, D. Wandke, W. Maus-Friedrichs, G. Däschlein, Clinical Plasma Medicine 2013, 1, 24.

[5]    A. Schmidt, S. Dietrich, A. Steuer, K.-D. Weltmann, T. von Woedtke, K. Masur, K. Wende, Journal of Biological Chemistry 2015, 290, 6731.

[6]    G. Isbary, G. Morfill, H. Schmidt, M. Georgi, K. Ramrath, J. Heinlin, S. Karrer, M. Landthaler, T. Shimizu, B. Steffes, British Journal of Dermatology 2010, 163, 78.

[7]    F. Brehmer, H. Haenssle, G. Daeschlein, R. Ahmed, S. Pfeiffer, A. Görlitz, D. Simon, M. Schön, D. Wandke, S. Emmert, Journal of the European Academy of Dermatology and Venereology 2015, 29, 148; T. Kisch, A. Helmke, S. Schleusser, J. Song, E. Liodaki, F. H. Stang, P. Mailaender, R. Kraemer, Microvascular research 2016, 104, 55; S. Kubinova, K. Zaviskova, L. Uherkova, V. Zablotskii, O. Churpita, O. Lunov, A. Dejneka, Scientific Reports 2017, 7, 45183.

[8]    M. Keidar, Plasma Sources Science and Technology 2015, 24, 033001.

[9]    K. Wende, S. Straßenburg, B. Haertel, M. Harms, S. Holtz, A. Barton, K. Masur, T. von Woedtke, U. Lindequist, Cell biology international 2014, 38, 412.

[10]   H. Tanaka, M. Mizuno, S. Toyokuni, S. Maruyama, Y. Kodera, H. Terasaki, T. Adachi, M. Kato, F. Kikkawa, M. Hori, Physics of Plasmas 2015, 22, 122004.

[11]   M. Vandamme, E. Robert, S. Dozias, J. Sobilo, S. Lerondel, A. Le Pape, J.-M. Pouvesle, Plasma medicine 2011, 1, 27.

[12]   M. Schuster, C. Seebauer, R. Rutkowski, A. Hauschild, F. Podmelle, C. Metelmann, B. Metelmann, T. von Woedtke, S. Hasse, K.-D. Weltmann, Journal of Cranio-Maxillofacial Surgery 2016, 44, 1445.

[13]   S. Blackert, B. Haertel, K. Wende, T. von Woedtke, U. Lindequist, Journal of dermatological science 2013, 70, 173.

[14]   A. Schmidt, T. von Woedtke, S. Bekeschus, Oxidative medicine and cellular longevity 2016, 2016, 1.

[15]   N. Iqbal, N. Iqbal, Molecular biology international 2014, 2014, 1.

[16] J. Berlanga‑Acosta, J. Gavilondo‑Cowley, P. López‑Saura, T. González‑López, M. D. Castro‑Santana, E. López‑Mola, G. Guillén‑Nieto, L. Herrera‑Martinez, International wound journal 2009, 6, 331.

[17] J. Wang, J. Yin, Q. Yang, F. Ding, X. Chen, B. Li, X. Tian, Oncotarget 2016, 7, 76693.

[18] E. S. Henson, S. B. Gibson, Cellular signalling 2006, 18, 2089.

[19] C. M. Stoscheck, L. E. King, Cancer research 1986, 46, 1030.

[20] R. S. Herbst, International Journal of Radiation Oncology* Biology* Physics 2004, 59, S21.

[21] J. Lackmann, S. Baldus, E. Steinborn, E. Edengeiser, F. Kogelheide, S. Langklotz, S. Schneider, L. Leichert, J. Benedikt, P. Awakowicz, Journal of Physics D: Applied Physics 2015, 48, 494003.

[22] S. Choi, P. Attri, I. Lee, J. Oh, J.-H. Yun, J. H. Park, E. H. Choi, W. Lee, Scientific Reports 2017, 7, 1027.

[23] E. Takai, T. Kitamura, J. Kuwabara, S. Ikawa, S. Yoshizawa, K. Shiraki, H. Kawasaki, R. Arakawa, K. Kitano, Journal of Physics D: Applied Physics 2014, 47, 285403.

[24] N. Y. Babaeva, G. V. Naidis, Trends in Biotechnology 2017; A. Bogaerts, N. Khosravian, J. Van der Paal, C. C. Verlackt, M. Yusupov, B. Kamaraj, E. C. Neyts, Journal of Physics D: Applied Physics 2015, 49, 054002.

[25] A. Bogaerts, M. Yusupov, J. Van der Paal, C. C. Verlackt, E. C. Neyts, Plasma Processes and Polymers 2014, 11, 1156; E. C. Neyts, M. Yusupov, C. C. Verlackt, A. Bogaerts, Journal of Physics D: Applied Physics 2014, 47, 293001.

[26] M. Yusupov, A. Bogaerts, S. Huygh, R. Snoeckx, A. C. van Duin, E. C. Neyts, The Journal of Physical Chemistry C 2013, 117, 5993; M. Yusupov, E. Neyts, U. Khalilov, R. Snoeckx, A. Van Duin, A. Bogaerts, New Journal of Physics 2012, 14, 093043; M. Yusupov, E. C. Neyts, C. C. Verlackt, U. Khalilov, A. C. van Duin, A. Bogaerts, Plasma Processes and Polymers 2015, 12, 162.

[27] J. Van der Paal, C. Verlackt, M. Yusupov, E. Neyts, A. Bogaerts, Journal of Physics D: Applied Physics 2015, 48, 155202.

[28] N. Khosravian, B. Kamaraj, E. Neyts, A. Bogaerts, Scientific reports 2016, 6, 19466.

[29] M. Yusupov, E. Neyts, P. Simon, G. Berdiyorov, R. Snoeckx, A. Van Duin, A. Bogaerts, Journal of Physics D: Applied Physics 2013, 47, 025205; C. Verlackt, E. Neyts, A. Bogaerts, Journal of Physics D: Applied Physics 2017, 50, 11LT01.

[30] C. Verlackt, E. Neyts, T. Jacob, D. Fantauzzi, M. Golkaram, Y. Shin, A. van Duin, A. Bogaerts, New Journal of Physics 2015, 17, 103005.

[31] N. Khosravian, A. Bogaerts, S. Huygh, M. Yusupov, E. C. Neyts, Biointerphases 2015, 10, 029501.

[32] S. Uchida, T. Yoshida, F. Tochikubo, Journal of Physics D: Applied Physics 2017, 50, 395203.

[33] M. Yusupov, K. Wende, S. Kupsch, E. Neyts, S. Reuter, A. Bogaerts, Scientific Reports 2017, 7, 5761.

[34] N. Y. Babaeva, N. Ning, D. B. Graves, M. J. Kushner, Journal of Physics D: Applied Physics 2012, 45, 115203.

[35] M. Yusupov, J. Van der Paal, E. Neyts, A. Bogaerts, Biochimica et Biophysica Acta (BBA)-General Subjects 2017, 1861, 839.

[36] J. Van der Paal, C. Verheyen, E. C. Neyts, A. Bogaerts, Scientific reports 2017, 7, 39526; J. Van der Paal, E. C. Neyts, C. C. Verlackt, A. Bogaerts, Chemical Science 2016, 7, 489.

[37] J. Razzokov, M. Yusupov, S. Vanuytsel, E. C. Neyts, A. Bogaerts, Plasma Processes and Polymers 2017, e1700013.

[38] H.-W. Huang, S. K. Mohan, C. Yu, Biochemical and biophysical research communications 2010, 402, 705.

[39] http://www.uniprot.org/uniprot/Q6QBS2.

[40] M. Abraham, D. van der Spoel, E. Lindahl, B. Hess, There is no corresponding record for this reference 2016; M. J. Abraham, T. Murtola, R. Schulz, S. Páll, J. C. Smith, B. Hess, E. Lindahl, SoftwareX 2015, 1, 19; D. Van Der Spoel, E. Lindahl, B. Hess, G. Groenhof, A. E. Mark, H. J. Berendsen, Journal of computational chemistry 2005, 26, 1701.

[41] N. Schmid, A. P. Eichenberger, A. Choutko, S. Riniker, M. Winger, A. E. Mark, W. F. van Gunsteren, European biophysics journal 2011, 40, 843.

[42] D. Petrov, C. Margreitter, M. Grandits, C. Oostenbrink, B. Zagrovic, PLoS computational biology 2013, 9, e1003154; C. Margreitter, M. M. Reif, C. Oostenbrink, Journal of computational chemistry 2017, 38, 714.

[43] D. Frishman, P. Argos, Proteins: Structure, Function, and Bioinformatics 1995, 23, 566.

[44] W. Humphrey, A. Dalke, K. Schulten, Journal of molecular graphics 1996, 14, 33.

[45] R. Chen, L. Li, Z. Weng, Proteins: Structure, Function, and Bioinformatics 2003, 52, 80; B. G. Pierce, Y. Hourai, Z. Weng, PloS one 2011, 6, e24657.

[46] H. Ogiso, R. Ishitani, O. Nureki, S. Fukai, M. Yamanaka, J.-H. Kim, K. Saito, A. Sakamoto, M. Inoue, M. Shirouzu, Cell 2002, 110, 775.

[47] S. Genheden, U. Ryde, Expert Opin Drug Discov 2015, 10, 449.

[48] N. Bibinov, P. Rajasekaran, P. M. D. Wandke, W. Viöl, P. Awakowicz, in *Biomedical engineering, trends in materials science*, InTech, 2011.

[49] S. Baldus, D. Schröder, N. Bibinov, V. Schulz-von der Gathen, P. Awakowicz, Journal of Physics D: Applied Physics 2015, 48, 275203.

[50] S. Baldus, F. Kogelheide, N. Bibinov, K. Stapelmann, P. Awakowicz, Journal of Physics D: Applied Physics 2015, 48, 375202.

[51] F. Kogelheide, K. Kartaschew, M. Strack, S. Baldus, N. Metzler-Nolte, M. Havenith, P. Awakowicz, K. Stapelmann, J.-W. Lackmann, Journal of Physics D: Applied Physics 2016, 49, 084004.

[52] S. Prestrelski, T. Arakawa, C. Wu, K. O'Neal, K. Westcott, L. Narhi, Journal of Biological Chemistry 1992, 267, 319.

[53] Y. N. Chirgadze, N. Nevskaya, Biopolymers 1976, 15, 607; A. Barth, Biochimica et Biophysica Acta (BBA)-Bioenergetics 2007, 1767, 1073.

[54] H.-S. Lu, J.-J. Chai, M. Li, B.-R. Huang, C.-H. He, R.-C. Bi, Journal of Biological Chemistry 2001, 276, 34913.

[55] L. O. NARHI, T. ARAKAWA, M. D. MCGINLEY, M. F. ROHDE, K. R. WESTCOTT, Chemical Biology & Drug Design 1992, 39, 182.

[56] C. Klinkhammer, C. Verlackt, F. Kogelheide, A. Bogaerts, N. Metzler-Nolte, K. Stapelmann, M. Havenith, J.-W. Lackmann, Scientific reports 2017, 7, 13828.

[57] A. M. Hirst, F. M. Frame, N. J. Maitland, D. O'Connell, BioMed research international 2014, 2014, 1.

[58] G. Daeschlein, O. Assadian, L. C. Kloth, C. Meinl, F. Ney, A. Kramer, Wound repair and regeneration 2007, 15, 399.

[59] M. Dezest, L. Chavatte, M. Bourdens, D. Quinton, M. Camus, L. Garrigues, P. Descargues, S. Arbault, O. Burlet-Schiltz, L. Casteilla, Scientific reports 2017, 7, 41163; A. Hirst, M. Simms, V. Mann, N. Maitland, D. O'connell, F. Frame, British journal of cancer 2015, 112, 1536.